Instability zones for isotropic and anisotropic multibladed rotor configurations.

Leonardo Sanches, Guilhem Michon, Alain Berlioz, Daniel Alazard

▶ **To cite this version:**

Leonardo Sanches, Guilhem Michon, Alain Berlioz, Daniel Alazard. Instability zones for isotropic and anisotropic multibladed rotor configurations.. Mechanism and Machine Theory, 2011, 46 (8), pp.1054-1065. 10.1016/j.mechmachtheory.2011.04.005 . hal-01852901

HAL Id: hal-01852901
https://hal.science/hal-01852901

Submitted on 2 Aug 2018

HAL is a multi-disciplinary open access archive for the deposit and dissemination of scientific research documents, whether they are published or not. The documents may come from teaching and research institutions in France or abroad, or from public or private research centers.

L'archive ouverte pluridisciplinaire **HAL**, est destinée au dépôt et à la diffusion de documents scientifiques de niveau recherche, publiés ou non, émanant des établissements d'enseignement et de recherche français ou étrangers, des laboratoires publics ou privés.

OATAO
Open Archive Toulouse Archive Ouverte

Open Archive Toulouse Archive Ouverte (OATAO)

OATAO is an open access repository that collects the work of Toulouse researchers and makes it freely available over the web where possible.

This is an author -deposited version published in: http://oatao.univ-toulouse.fr/
Eprints ID: 4923

To link to this article: DOI: 10.1016/j.mechmachtheory.2011.04.005

URL: http://dx.doi.org/10.1016/j.mechmachtheory.2011.04.005

To cite this version: SANCHES Leonardo, MICHON Guilhem, BERLIOZ Alain, ALAZARD Daniel. Instability zones for isotropic and anisotropic multibladed rotor configurations. *Mechanism and Machine Theory*, vol. 46, n° 8, pp. 1054-1065.
ISSN 0094-114X

Any correspondence concerning this service should be sent to the repository administrator:
staff-oatao@inp-toulouse.fr

Instability zones for isotropic and anisotropic multibladed rotor configurations

Leonardo Sanches [a,*], Guilhem Michon [a], Alain Berlioz [b], Daniel Alazard [c]

[a] Université de Toulouse, ICA, ISAE, 10 Av. Edouard Belin, Toulouse, France
[b] Université de Toulouse, ICA, UPS, 10118 Route de Narbonne, Toulouse, France
[c] Université de Toulouse, DMIA,ISAE, 10 Av. Edouard Belin, Toulouse, France

Keywords:
Ground resonance
Nonlinear dynamics
Floquet Theory
Isotropic rotors
Anisotropic rotors

A B S T R A C T

Helicopter ground resonance is an unstable dynamic phenomenon which can lead to the total destruction of the aircraft during take-off or landing phases. The earliest research in this domain was carried out by Coleman and Feingold during the decade of 60s. The instability was predicted by using classical procedures once the rotor was considered as isotropic, consequently, the periodic equations of motion could be simplified to a system with constant coefficients by introducing a change of variables, known as the Coleman Variable Transformation. The goal of the present work is to further comprehend the phenomenon and the influence of the anisotropic properties of rotors by analyzing the periodic set of equations of motion. For this, Floquet's Theory (Floquet's Method — FM) is used. The analysis for predicting the ground resonance phenomenon in isotropic and anisotropic rotor configurations is explored. The conclusions lead to verify the appearance of bifurcation points depending on the anisotropic characteristic present in the rotor. The temporal response analysis in the motion of helicopter with one asymmetric blade at unstable regions highlighted the presence of non symmetric rotor deformation shapes.

Contents

* Corresponding author. Tel.: +33 5 61 33 89 59; fax: +33 5 61 33 83 52.
E-mail addresses: leonardo.sanches@isae.fr (L. Sanches), guilhem.michon@isae.fr (G. Michon), berlioz@cict.fr (A. Berlioz), daniel.alazard@isae.fr (D. Alazard).

1. Introduction

The stability of the helicopter dynamics on ground was first studied by Coleman and Feingold [1]. They observed that the ground resonance phenomenon consists of a self-excited oscillation caused by the interaction between the lagging motion of the rotor blades and other modes of helicopter motion. The prediction of the unstable regions with isotropic rotor configurations was easily achieved once the periodic characteristics of the governing equations of motion disappeared by a change of variables. This process, applicable only to isotropic rotors, is identified as the Coleman Transformation and more generally the multi blade coordinate transformation.

Later on, research works were carried out to verify the influence of the air resonance on the stability of helicopters on ground [2,3]. Major contributions in understanding the ground resonance phenomenon in hingeless and bearingless rotors were made by Army researchers, for example, Dawson [4] and Hodges [5].

Recently, the influence of nonlinear springs and dampers on the instability zones was analyzed by Kunz [6]. Byers and Gandhi [7] explored the passive control of the problem. Also, Duchemin [8] studied the dynamic behavior of flexible rotors in onboard systems.

In all the above mentioned works, only symmetric rotors have been examined. Nevertheless, the study of anisotropic rotors is very interesting from a practical point of view. Indeed, due to aging, the properties of stiffness and damping can vary from one blade to another.

With the objective of further understanding the ground resonance phenomenon, the analysis is extended to verify the influence of dissimilarities in blades on the stability of the phenomenon. For this, Coleman Transformation is no more valid, therefore, the treatment of the periodic equations of motion is envisioned.

By keeping the periodic terms in the equations, Floquet's Theory [9] (Floquet's Method — FM) was employed to carry out the stability analysis of helicopters with isotropic rotor and the results were compared with those obtained by applying the Coleman Transformation [10]. Also, Chopra and Wang [11] have studied the effects of blade dissimilarities. However they considered few examples and small dissimilarities on the analysis.

The same theory was applied to the vibration analysis of asymmetric rotating machines [12,13] and on the dynamic system with parametric excitations [14].

Moreover, new routs of research have been introduced recently by an extension of Floquet's Theory to treat time-delayed models of dynamical systems with parametric excitations [15,16].

The present paper uses the Floquet Theory to predict and study the ground resonance phenomenon through illustrations of stability maps for isotropic and anisotropic rotors. A wide range of anisotropic rotors were considered and high level of blade asymmetries.

A mechanical model which is used to develop the dynamic equations of motion is presented in Section 2. In Section 3, the applied methodology – Floquet's Method – is briefly described. In Sections 4 and 5, the predicted critical rotor speeds are presented for an isotropic and anisotropic rotor and compared.

1.1. Nomenclatures

a	$[m]$	Rotor eccentricity
b	$[m]$	Blade length
$\mathbf{F_{ext}}$		External force vector
G, K, M		Damping, stiffness and mass matrix of the dynamical system
Iz_{b_k}	$[kg\,m^2]$	Lag rotational inertia of the kth blade around its center of gravity
K_{b_k}	$[N\,m]$	k^{th} blade lead-lag stiffness
K_{f_X}, K_{f_Y}	$[N\,m^{-1}]$	Longitudinal and transversal stiffness of fuselage
m_f, m_{b_k}	$[kg]$	Fuselage mass and mass of k^{th} blade
r_{a_k}		$\sqrt{ar_{b_k}}$
r_{m_k}	$[m]$	Ratio between the static moment of the kth blade over the total mass of the helicopter
r_{b_k}	$[m^{-1}]$	Ratio between the static moment over the total lead-lag rotational inertia of the kth blade
S, v		State matrix and vector of Eq. (4)
u		General variables
$x(t)$, $y(t)$	$[m]$	Longitudinal and transversal displacement of the fuselage
x_{b_x}, y_{b_x}	$[m]$	Blade's position in x and y directions
(x, y, z)		Mobile coordinate system attached to the rotor hub
(X_0, Y_0, Z_0)		Inertial referential system
GREEK LETTERS		
$\varphi_k(t)$	$[rad]$	Lead-lag angle of k^{th} blade
Φ		Transition Matrix (Floquet's Theory)
λ		Characteristic multipliers
θ_k	$[rad]$	Azimuth angle for the k^{th} blade
ω_{b_k}	$[rad\,s^{-1}]$	Lag resonance frequency of the kth blade at $\Omega = 0$
ω_x, ω_y	$[rad\,s^{-1}]$	Fuselage's resonance frequencies in x and y directions
Ω	$[rad\,s^{-1}]$	Rotor speed

2. Mechanical model

Similar to that proposed by Coleman and Feingold, the present mechanical model is developed to characterize the dynamic behavior of a helicopter with a hinged rotor. In other words, it consists of figuring out the relation between the longitudinal – $x(t)$– and lateral displacement – $y(t)$ – of the fuselage, and the k^{th} blade lag angle – φ_k (t) – in terms of the rotor speed Ω and time t. Fig. 1 illustrates a general schema of the system.

The fuselage is considered to be a rigid body with its center of gravity at point O. At the initial time, the origin of an inertial coordinate system (X_0,Y_0,Z_0) is coincident at this point. The body is connected to springs which represent the flexibility of the landing skid.

The rotor head system consists of an assembly of one rigid rotor hub with Nb blades. Each blade is represented by a concentrated mass located at a distance b from the lag articulation (point B) and, on each articulation, a torsional spring is present. The origin of a mobile coordinate system (x, y, z), parallel to the inertial one, is located at the geometric center of the rotor hub (point A). Both, body and rotor head, are joined by a rigid shaft, the aerodynamical forces on the blades are neglected and any viscous damping is taken into account.

2.1. The governing equations of motion

In order to obtain the governing equations of motion, following assumptions are made:

- The fuselage has a mass m_f and the spring stiffness connected to it K_{f-X} and K_{f-Y} through x and y directions, respectively;
- The rotor is composed of $Nb=4$ blades and each blade k has an azimuth angle of $\theta_k=2\pi(k-1)/Nb$ with the x-axis;
- Each blade has the same mass m_{b_k} and moment of inertia around the vertical axis is Iz_{b_k};
- The angular spring stiffness for each k blade is K_{b_k};
- The k^{th} blade position projected in the inertial coordinate system is:

$$x_{b\_k} = a\cos(\Omega t + \theta_k) + b\cos(\Omega t + \theta_k + \varphi_k(t)) + x(t) \tag{1}$$

$$y_{b\_k} = a\sin(\Omega t + \theta_k) + b\sin(\Omega t + \theta_k + \varphi_k(t)) + y(t) \tag{2}$$

where a is the hinge offset.

The general variable $\mathbf{u}$, which corresponds to the degrees of freedom of the system, is considered as follows,

$$\{\ \mathbf{u}_{1..6}(t)\} = \{\ x(t)\quad y(t)\quad \varphi_1(t)\quad \varphi_2(t)\quad \varphi_3(t)\quad \varphi_4(t)\ \} \tag{3}$$

The equations of motion are then obtained by applying Lagrange equation to the kinetic and potential energy expressions of the system, given in Appendix A.

These equations are obtained by following a first order Taylor's series expansion of the trigonometric blade lead-lag angle terms and then only the linear terms are considered. In a matrix form, these equations are presented as below,

$$\mathbf{M}\ddot{\mathbf{u}} + \mathbf{G}\dot{\mathbf{u}} + \mathbf{K}\mathbf{u} = \mathbf{F}_{ext} \tag{4}$$

where $\mathbf{M}$, $\mathbf{G}$ and $\mathbf{K}$ are the linear periodic mass, damping and stiffness matrices, respectively. These are non-symmetric and non-diagonal matrices due to the presence of parametric terms. Moreover, F_{ext} is the external force vector which is equal to zero for an isotropic rotor configuration. All of these matrices are given in Eqs. (5)–(8), in the following.

$$\mathbf{M} = \begin{bmatrix} 1 & 0 & -r_{m_1}\sin(\Omega t+\theta_1) & -r_{m_2}\sin(\Omega t+\theta_2) & -r_{m_3}\sin(\Omega t+\theta_3) & -r_{m_4}\sin(\Omega t+\theta_4) \\ 0 & 1 & r_{m_1}\cos(\Omega t+\theta_1) & r_{m_2}\cos(\Omega t+\theta_2) & r_{m_3}\cos(\Omega t+\theta_3) & r_{m_4}\cos(\Omega t+\theta_4) \\ -r_{b_1}\sin(\Omega t+\theta_1) & r_{b_1}\cos(\Omega t+\theta_1) & 1 & 0 & 0 & 0 \\ -r_{b_2}\sin(\Omega t+\theta_2) & r_{b_2}\cos(\Omega t+\theta_2) & 0 & 1 & 0 & 0 \\ -r_{b_3}\sin(\Omega t+\theta_3) & r_{b_3}\cos(\Omega t+\theta_3) & 0 & 0 & 1 & 0 \\ -r_{b_4}\sin(\Omega t+\theta_4) & r_{b_4}\cos(\Omega t+\theta_4) & 0 & 0 & 0 & 1 \end{bmatrix} \tag{5}$$

$$\mathbf{G} = \begin{bmatrix} 0 & 0 & -2\Omega\, r_{m_1}\cos(\Omega t+\theta_1) & -2\Omega\, r_{m_2}\cos(\Omega t+\theta_2) & -2\Omega\, r_{m_3}\cos(\Omega t+\theta_3) & -2\Omega\, r_{m_4}\cos(\Omega t+\theta_4) \\ 0 & 0 & -2\Omega\, r_{m_1}\sin(\Omega t+\theta_1) & -2\Omega\, r_{m_2}\sin(\Omega t+\theta_2) & -2\Omega\, r_{m_3}\sin(\Omega t+\theta_3) & -2\Omega\, r_{m_4}\sin(\Omega t+\theta_4) \\ 0 & 0 & 0 & 0 & 0 & 0 \\ 0 & 0 & 0 & 0 & 0 & 0 \\ 0 & 0 & 0 & 0 & 0 & 0 \\ 0 & 0 & 0 & 0 & 0 & 0 \end{bmatrix} \tag{6}$$

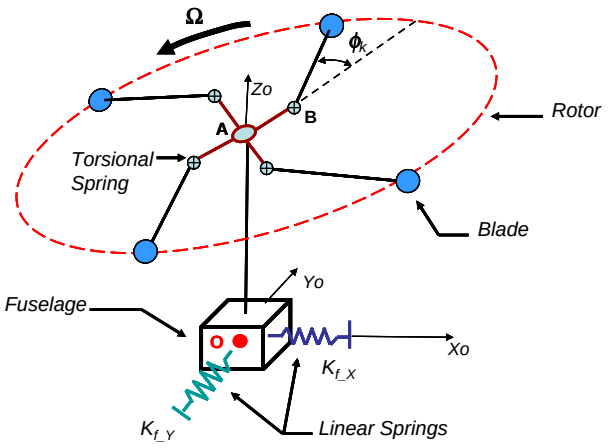

Fig. 1. General schema of the mechanical model.

$$\mathbf{K} = \begin{bmatrix} \omega_x^2 & 0 & \Omega^2 r_{m_1}\sin(\Omega t+\theta_1) & \Omega^2 r_{m_2}\sin(\Omega t+\theta_2) & \Omega^2 r_{m_3}\sin(\Omega t+\theta_3) & \Omega^2 r_{m_4}\sin(\Omega t+\theta_4) \\ 0 & \omega_y^2 & -\Omega^2 r_{m_1}\cos(\Omega t+\theta_1) & -\Omega^2 r_{m_2}\cos(\Omega t+\theta_2) & -\Omega^2 r_{m_3}\cos(\Omega t+\theta_3) & -\Omega^2 r_{m_4}\cos(\Omega t+\theta_4) \\ 0 & 0 & \omega_{b_1}^2+\Omega^2 r_{a_1}^2 & 0 & 0 & 0 \\ 0 & 0 & 0 & \omega_{b_2}^2+\Omega^2 r_{a_2}^2 & 0 & 0 \\ 0 & 0 & 0 & 0 & \omega_{b_3}^2+\Omega^2 r_{a_3}^2 & 0 \\ 0 & 0 & 0 & 0 & 0 & \omega_{b_4}^2+\Omega^2 r_{a_4}^2 \end{bmatrix} \tag{7}$$

$$\mathbf{F}_{ext} = \begin{bmatrix} \sum_{k=1}^{Np}\Omega^2 r_{m_k}\left(\frac{a+b}{b}\right)\cos(\Omega t+\theta_k) \\ \sum_{k=1}^{Np}\Omega^2 r_{m_k}\left(\frac{a+b}{b}\right)\sin(\Omega t+\theta_k) \\ 0 \\ 0 \\ 0 \\ 0 \end{bmatrix} \tag{8}$$

where

$$r_{m_k} = \frac{b\, m_{b\_k}}{m_f + \sum_{k=1}^{Np} m_{b\_k}}, \quad r_{b_k} = \frac{b\, m_{b\_k}}{b^2\ m_{b\_k} + Iz_{b\_k}}, \quad r_{a_k}^2 = a\ r_{b_k}$$

$$\omega_x^2 = \frac{K_{f\_X}}{m_f + \sum_{k=1}^{Np} m_{b\_k}}, \quad \omega_y^2 = \frac{K_{f\_Y}}{m_f + \sum_{k=1}^{Np} m_{b\_k}}, \quad \omega_{b_k}^2 = \frac{K_{b\_k}}{b^2\ m_{b\_k} + Iz_{b\_k}} \quad k = 1..Np.$$

It is noted that r_{m_k} and r_{b_k} factors, which represent the ratio between the blade static moment over the total inertial mass of the helicopter and the total rotational inertia of the blade, respectively, are smaller when compare to unity.

The terms ω_x and ω_y are the resonance frequencies of the fuselage in the x and y directions, respectively. Moreover, $\omega_{b_{3..6}}$ are the lead-lag resonance frequencies of blades 1 to 4.

Table 1
Numerical values of the fuselage and rotor head inputs.

Fuselage			Rotor	
$m_f = 2902.9$ [kg]		$m_b = 31.9$ [kg]	$a = 0.2$ [m]	$b = 2.5$ [m]
$\omega_x = 3$ [Hz]	$\omega_y = 3$ [Hz]	$\omega_b = 1.5$ [Hz]	$I_{zb} = 259$ [kg m^2]	

3. Floquet's method

In this section, a stability analysis of the periodic equations of motion is carried out in order to determine the critical rotor speeds at which the unstable oscillations in helicopter may appear. The Floquet's Theory is used.

Representing the dynamical system in a state-space format and considering **S**(t) the state-space matrix with period T of Eq. (4), the system becomes,

$$\begin{aligned} &\dot{\mathbf{v}}(t) = \mathbf{S}(t)\mathbf{v}(t), \quad t > t_0 \\ &\mathbf{v}(t_0) = \mathbf{v}_0, \quad \mathbf{v}(t) = \begin{bmatrix} \mathbf{u}(t) & \dot{\mathbf{u}}(t) \end{bmatrix}^T \end{aligned} \tag{9}$$

where $\mathbf{v}(t)$ is the state variable.

By Floquet's Theory, a transition matrix Φ, which relates $\mathbf{v}(t)$ with $\mathbf{v}(t_0)$, is defined as,

$$\Phi(t, t_0) = \mathbf{P}(t, t_0)\, e^{(t-t_0)\,\mathbf{Q}}. \tag{10}$$

The monodromy matrix **R** or the Floquet Transition Matrix (FTM), defined as $\mathbf{R} = \Phi(t_0 + T, t_0)$ is computed by admitting the periodic system in Eq. (4) as a switched periodical system. As reported Berlioz et al. [14], the matrix **S**(t) is approximated by a series of p step functions over the period T and the monodromy matrix is then obtained as,

$$\mathbf{R} = \prod_{k=1}^{p} \exp(\mathbf{S}_k \Delta t) \tag{11}$$

where $\mathbf{S}_k$, within the interval $\Delta t = t_k - t_{k-1}$, is constant and defined at $\mathbf{S}(t_{k-1})$.

The dynamical system Eq. (4) is exponentially stable if **R** is Schurz. It means that the norm of the eigenvalues (λ) of **R,** known as characteristic multipliers, is smaller than unity.

4. Numerical results

This section aims at predicting the boundaries of critical regions at which the system is unstable for one isotropic and a wide range of anisotropic rotor configurations. For this the Floquet's Method is used.

4.1. Isotropic rotor configuration

The numerical values used for the system's inputs are defined in Table 1. It is important to notice that the subscript k in the terms is eliminated once the rotor is isotropic.

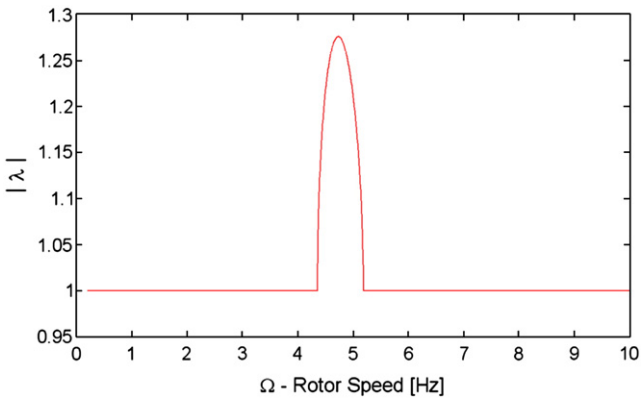

Fig. 2. Evolution of the characteristic multipliers as function of the rotor speed.

Table 2
Limits of instability zones predicted by the Floquet's Method in Hz.

Critical rotor speed	Limits of instability zone [Hz]	
Floquet	4.35	5.18
Coleman	4.357	5.187

For every rotating speed defined between 0 and 10 Hz by a step of 0.02 Hz, the FM is applied and the characteristic multipliers are obtained. Fig. 2 presents the evolution of biggest norm value of the characteristic multipliers with respect to the speed of rotation. The period T is divided in $p = 64$ parts.

Once the instability zone is determined through Fig. 2, the boundary limits (beginning and ending points) of the region are then collected and presented in Table 2.

Considering the Coleman Transformation expressions described in Ref. [10] and applying them on Eq. (4), the final equations of motions and the criteria of stability are presented in Appendix B.

Using the data defined in Table 1 and analyzing the stability of the dynamical system for every rotating speed varying from 0 to 10 Hz by a step of 0.02 Hz, the instability zone is identified and the boundary limits found are joined in Table 2 with those obtained by using FM.

Both methods give the same instability zone.

4.2. Anisotropic rotor configuration

The interest of this subsection is to determine the instability zones where the dynamical system becomes unstable for anisotropic rotors by using the method described in Section 3.

The numerical values used for the system's inputs are the same as those defined in Table 1, except for the lead-lag resonance frequencies of blades ω_{b_k}. In Case study 1, only one blade is modified. Finally, for Cases 2 and 3, two blades are altered by considering them in adjacent and opposite locations, respectively.

- Case 1:
  Three blades are considered having the same lead-lag resonance frequency equal to 1.5 Hz, while the last one is varied from -100% to $+100\%$ by a step of 9% of the blade lead-lag frequency indicated previously.
  Similar to the procedure applied for an isotropic rotor and for each specific case of anisotropy, FM is applied. The evolution of the characteristic multipliers along with the rotor speed is obtained, the instability zones are determined and only the boundary speeds are collected. The same value for $p = 64$ parts is considered.
  Fig. 3 shows the evolution of unstable regions as a function of the rotor speed and the asymmetry parameter ($\Delta\omega_4$).
- Case 2:
  In this case, two adjacent blades (3rd and 4th blades) have been altered from -100 to $+100\%$ by a step of 9% of the reference value of 1.5 Hz which is the blade lead-lag resonance frequency considered for the other blades.
  By repeating the procedure used in Case study 1, Fig. 4 illustrates tri-dimensionally the limits of the instability zones as function of the adjusting parameters and the rotor speed. The gray color represents the unstable regions.
  Introducing different constant values for ω_{b_3} (-100%, -52.381%, 52.381% and 100%), Fig. 5 shows the evolution of the instabilities zones as function of $\Delta\omega_{b_4}$ for each rotor configuration, similar to the procedure used in Case 1.

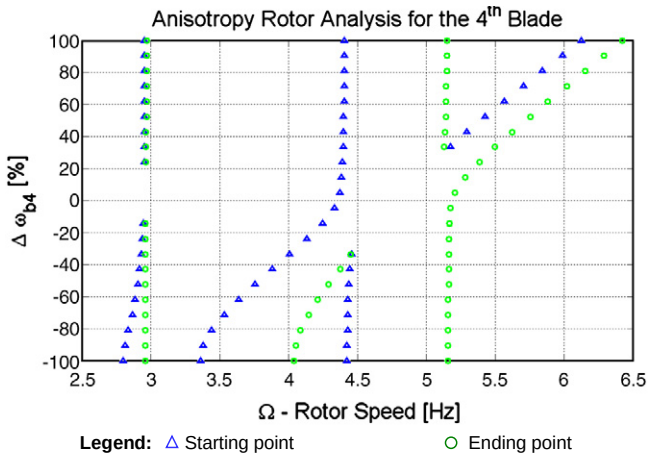

Fig. 3. Helicopter stability analysis by considering asymmetries on the 4th blade.

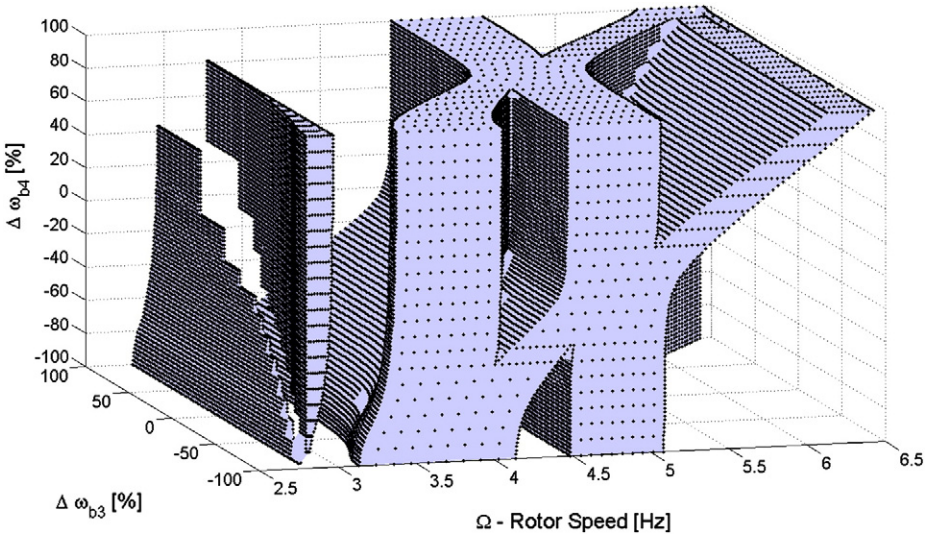

Fig. 4. Helicopter stability analysis by considering asymmetries on the 3rd and 4th blades.

- Case 3:
  In this case, the same procedure is carried out as discussed previously. However, the blades which have been modified are in opposite positions (2nd and 4th blades). Fig. 6 illustrates, tri-dimensionally, the limits of the instability zones as a function of $\Delta\omega_{b_2}$ and $\Delta\omega_{b_4}$.
  Moreover, assuming constant values for ω_{b_2} (-100%, -52.381%, 52.381% and 100%), as in previous case, Fig. 7 illustrates the evolution of the instabilities zones as function a of $\Delta\omega_{b_4}$.

5. Discussion

Regarding the stability analysis for isotropic helicopter as in Fig. 2, the results highlight the presence of unstable oscillations at $4.35 \leq \Omega \leq 5.18$ Hz. Chopra in his work [11] explained that this instability is due to the coalescence frequencies between fuselage and an asymmetric rotor mode shape (forward whirling mode) at a specific range of the rotor speed.

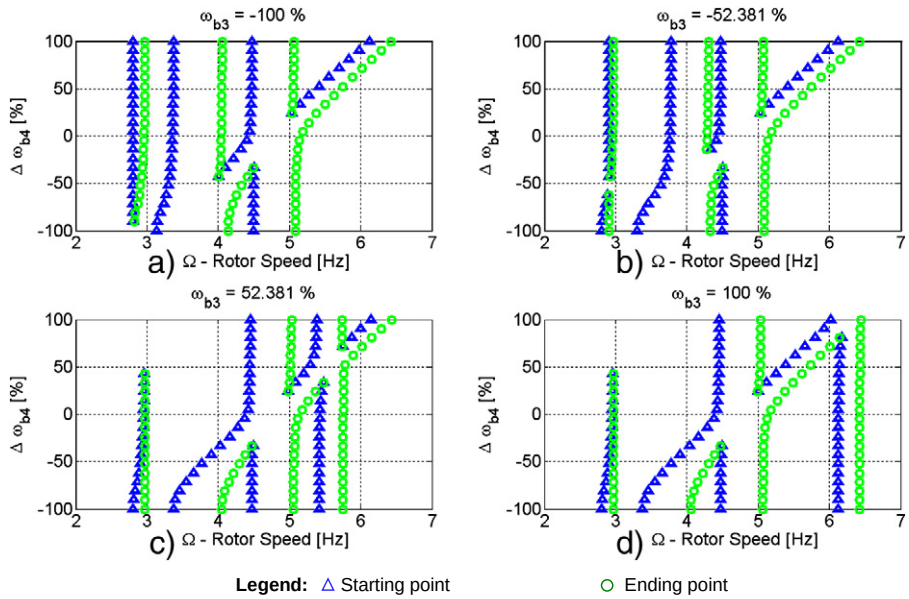

Fig. 5. Anisotropic rotor analysis for the 4th blades considering different values of ω_{b_3}.

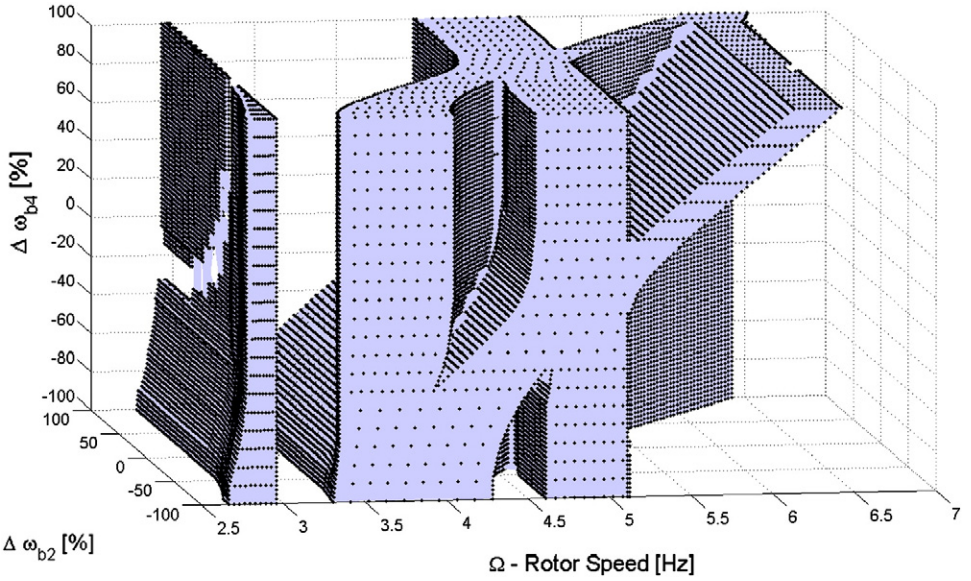

Fig. 6. Helicopter stability analysis by considering asymmetries on the 2nd and 4th blades.

Considering the influence of asymmetries in one blade in Case 1, Fig. 3 illustrates the presence of a main instability region at $4.4 \leq \Omega \leq 5.2$ Hz which is not altered for almost all values of $\Delta\omega_{b_4}$. It corresponds exactly to the same critical region found for an isotropic rotor.

Also, another unstable region is observed at low rotor speeds for a wide range of asymmetries blade. The critical rotating speed is around 3 Hz which corresponds to the natural frequency of the fuselage.

Nevertheless, the two braches come out from the main region defining the evolution of instability zones as function of blade dissimilarity ($\Delta\omega_{b_4}$). This is shown in the figure like an "x" shape with the main instability region.

Referring to the specific case where $\Delta\omega_{b_4} = -60\%$, Fig. 8 illustrates the deformation shapes of helicopter at the instants of maximal amplitudes of longitudinal and lateral displacement of the fuselage for each unstable regions. These deformation shapes are obtained from the temporal responses by using a numerical step-by-step integration method (see Appendix C).

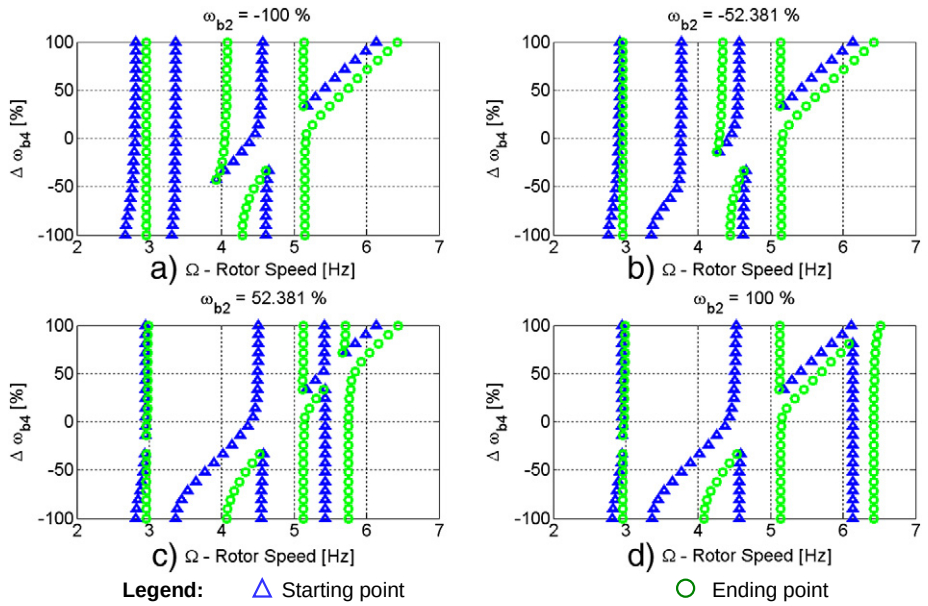

Fig. 7. Anisotropic rotor analysis for the 4th blades considering different values of ω_{b_2}.

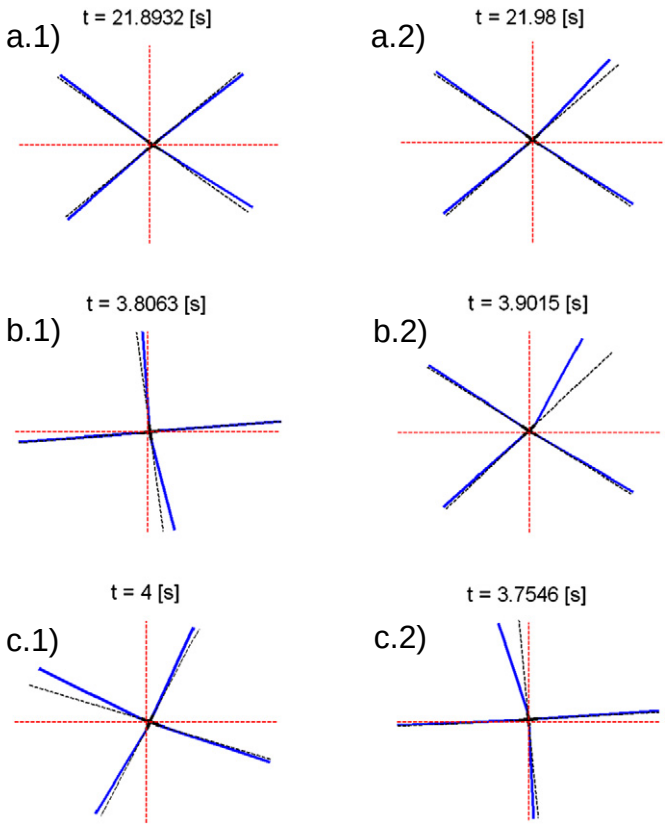

Fig. 8. Deformation shapes of an ($\Delta\omega_{b_4} = -60\%$) for Ω, in Hz, equal to a) 2.929 Hz, b) 3.945 and c) 4.797 at the maximum 1) longitudinal and 2) lateral displacement.

In order to help the visualization of the figure, a gain of 40 in case a) and 20 in remainder cases are applied in all deformation amplitudes. The intersection point between two dashed red lines corresponds to the rest point of the helicopter and the dashed black lines indicate the level zero of blade lead-lag oscillations.

Moreover, from the analysis of deformation shapes and temporal responses, one verifies a non symmetric rotor deformation in all cases a) to c). For $\Omega = 2.929$ and 3.945 Hz, high oscillations of the dissymmetric blade are observed when compared to other blades. Nevertheless, the sine signals which describe the motion of blades present mean values different from zero in the first case; whereas, in the second case, are zero for all blades.

In case c) where $\Omega = 4.797$ Hz, the amplitude of motion of the dissymmetric blade is smaller than the others. One remarks also the highest amplitude of oscillations for the blade situated in opposition with respect to the asymmetric blade.

Regarding the influence of other blades dissimilarities (Cases 2 and 3), examining the obtained results and comparing to the first case, the same characteristics for the instability regions were obtained in both cases: a main region at $4.4 \leq \Omega \leq 5.2$ Hz, another at low speeds for almost all values of $\Delta\omega_{b_4}$ and two branches coming out of the main region.

Nevertheless, due to the changes in two blades, the appearance of a new main region is also detected which moves depending on the values attributed to $\Delta\omega_{b_3}$ or $\Delta\omega_{b_2}$. As they increase, the new region moves to high values of the rotor speed.

Small differences between Cases 2 and 3 can be found in the boundary values of the new main unstable region and in the instability zone at a low rotor speed.

6. Conclusions

For the comprehension and analysis of the ground resonance phenomenon in helicopter with lead-lag articulated bladed rotors, this paper focused on predicting the critical rotor speeds at which unstable oscillations may occur for an isotropic and wide range of anisotropic rotor configurations. For this, Floquet Theory was used.

For the isotropic rotor configuration, the numerical results showed one well defined instability zone at rotor speed values between 4.35 and 5.18 Hz.

However, in order to determine the influence of blade dissimilarities on the stability of ground resonance phenomenon in helicopters, three case studies were performed. For the first case only one blade was altered and, for the second and third cases, two blades in adjacent and in opposite positions, respectively, were modified.

The investigated asymmetries were achieved by varying the blade lead-lag resonance frequency in percentage from -100 to $+100$ related to the reference values of an isotropic rotor.

Maps of stability were determined for these types of rotors and a complex evolution of instability zones, beyond the appearance of new critical regions, was observed.

Nevertheless, similarities in the stability maps of helicopters with isotropic and anisotropic rotors were found. In all cases of anisotropic rotor configurations, the results verified the presence of the same instability zone found in the isotropic rotors.

Analysis on the deformation shapes on each unstable region of a helicopter with one asymmetric blade was carried out. The deformations, obtained from the temporal responses, highlighted the influence of the dissymmetric blade.

Regarding the similarities between dissymmetric rotors, a common critical region is observed at low values of the rotor speed. Moreover, small differences were noted between Case studies 2 and 3.

Appendix A

In the present section, the kinetic and potential energies expressions of the dynamical system are presented.

- Kinetic energies:
  The total kinetic energy T_{Tot} expression of the dynamical system are given as

$$T_{Tot} = T_{Fus} + T_{RH} \tag{A.1}$$

where T_{Fus} and T_{RH} are the kinetic energy expressions of the fuselage and rotor head system, respectively. These energy expressions are presented below as

$$T_{Fus} = \frac{m_f}{2}\left(\dot{x}^2 + \dot{y}^2\right) \tag{A.2}$$

$$T_{RH} = \frac{1}{2}\sum_{k=1}^{Np} m_{b_k}\left(\dot{x}_{b\_k}^2 + \dot{y}_{b\_k}^2\right) = \frac{1}{2}m_{b_k}\cdots$$
$$\sum_{k=1}^{Np}\left\{\begin{array}{c}\left(\dot{x}^2 + \dot{y}^2\right) + b^2\dot{\varphi}_k^2 + 2b^2\Omega\dot{\varphi}_k + b^2\Omega^2\left(a^2 + b^2\right)\\ 2ab\cos(\varphi_k)\left[\Omega^2 + \Omega\dot{\varphi}_k\right] + 2a\Omega\left[-\dot{x}\sin(\Omega t + \theta_k) + \dot{y}\cos(\Omega t + \theta_k)\right]\\ 2b(\Omega\dot{y} + \dot{y}\dot{\varphi}_k)\cos(\Omega t + \theta_k + \varphi_k) - 2b(\Omega\dot{x} + \dot{x}\dot{\varphi}_k)\sin(\Omega t + \theta_k + \varphi_k)\end{array}\right\}. \tag{A.3}$$

- Potential energies:
  The total potential energy U_{Tot} expression of the dynamical system are given as

$$U_{Tot} = U_{Fus} + U_{RH} \tag{A.4}$$

where U_{Fus} and U_{RH} are the potential energy expressions of the fuselage and rotor head system, respectively. These energy expressions are presented below as

$$U_{Fus} = \frac{1}{2}\left(K_{f-X}x^2 + K_{f-Y}y^2\right) \tag{A.5}$$

$$U_{RH} = \frac{1}{2}\sum_{k=1}^{Np} K_{b_k}\varphi_k^2. \tag{A.6}$$

Appendix B

In this appendix, the periodic equations of motion are transformed by using Coleman Transformation. The final governing equations are obtained and the criteria of stability are presented.

Once the Coleman Transformation [10], defined as:

$$\eta = -\left(\frac{2}{Np}\right)\sum \varphi_k \sin(\Omega t + \theta_k) \quad and \quad \zeta = -\left(\frac{2}{Np}\right)\sum \varphi_k \cos(\Omega t + \theta_k) \tag{B.1}$$

is applied on Eq. (4), the below a matrix differential equation is obtained.

$$\begin{bmatrix} 1 & 0 & r_m\, Np/2 & 0 \\ 0 & 1 & 0 & -r_m\, Np/2 \\ r_b & 0 & 1 & 0 \\ 0 & -r_b & 0 & 1 \end{bmatrix} \begin{Bmatrix} \ddot{x} \\ \ddot{y} \\ \ddot{\eta} \\ \ddot{\zeta} \end{Bmatrix} + \begin{bmatrix} 0 & 0 & 0 & 0 \\ 0 & 0 & 0 & 0 \\ 0 & 0 & 0 & -2\Omega \\ 0 & 0 & 2\Omega & 0 \end{bmatrix} \begin{Bmatrix} \dot{x} \\ \dot{y} \\ \dot{\eta} \\ \dot{\zeta} \end{Bmatrix} + \begin{bmatrix} \omega_x^2 & 0 & 0 & 0 \\ 0 & \omega_y^2 & 0 & 0 \\ 0 & 0 & \omega_b^2 - \Omega^2\left(1 - r_a^2\right) & 0 \\ 0 & 0 & 0 & \omega_b^2 - \Omega^2\left(1 - r_a^2\right) \end{bmatrix} \begin{Bmatrix} x \\ y \\ \eta \\ \zeta \end{Bmatrix} = \begin{Bmatrix} 0 \\ 0 \\ 0 \\ 0 \end{Bmatrix} \tag{B.2}$$

Note that the subscript k is eliminate from Eq. (4) once it is isotropic rotor.

The dynamical system in Eq. (B.1) is stable at a rotating speed Ω if the real part of all eigenvalues is defined negative [1,10].

Appendix C

Through a numerical step-by-step integration method ("Adams113") and by using MATLAB®, this section presents the temporal responses of a helicopter with one dissymmetric blade $\Delta\omega_{b_4} = -60\%$.

The rotating speeds values considered for the analyses correspond to the mean rotor speeds values at each unstable region observed in Fig. 3. They are, in Hz, equal to 2.929, 3.945 and 4.797.

The initial conditions imposed are 0.1° for the lead-lag oscillation of 4th blade, and zero for all remainder amplitudes and speeds.

Fig. C.1 illustrates the results obtained at each unstable region.

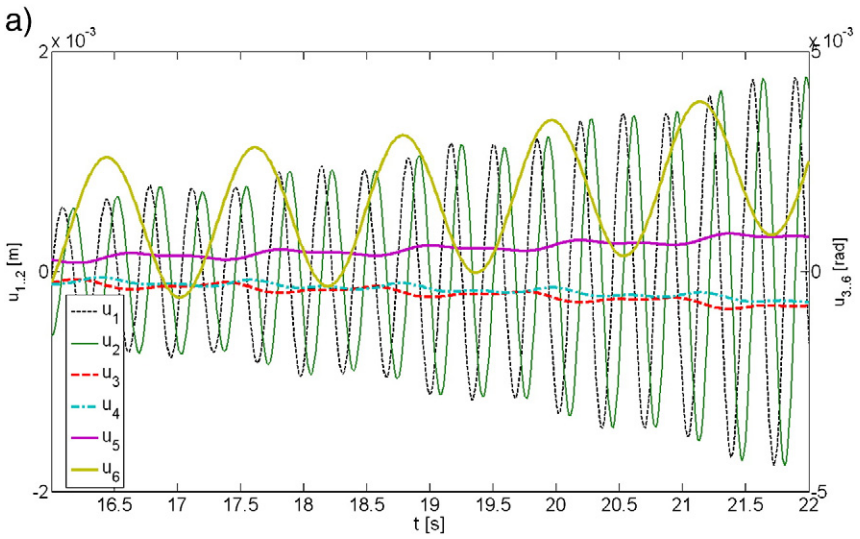

Fig. C.1. Temporal Responses at Ω, in Hz, equal to a) 2.929 Hz, b) 3.945 and c) 4.797 for a one blade dissymmetric helicopter ($\Delta\omega_{b_4} = -60\%$).

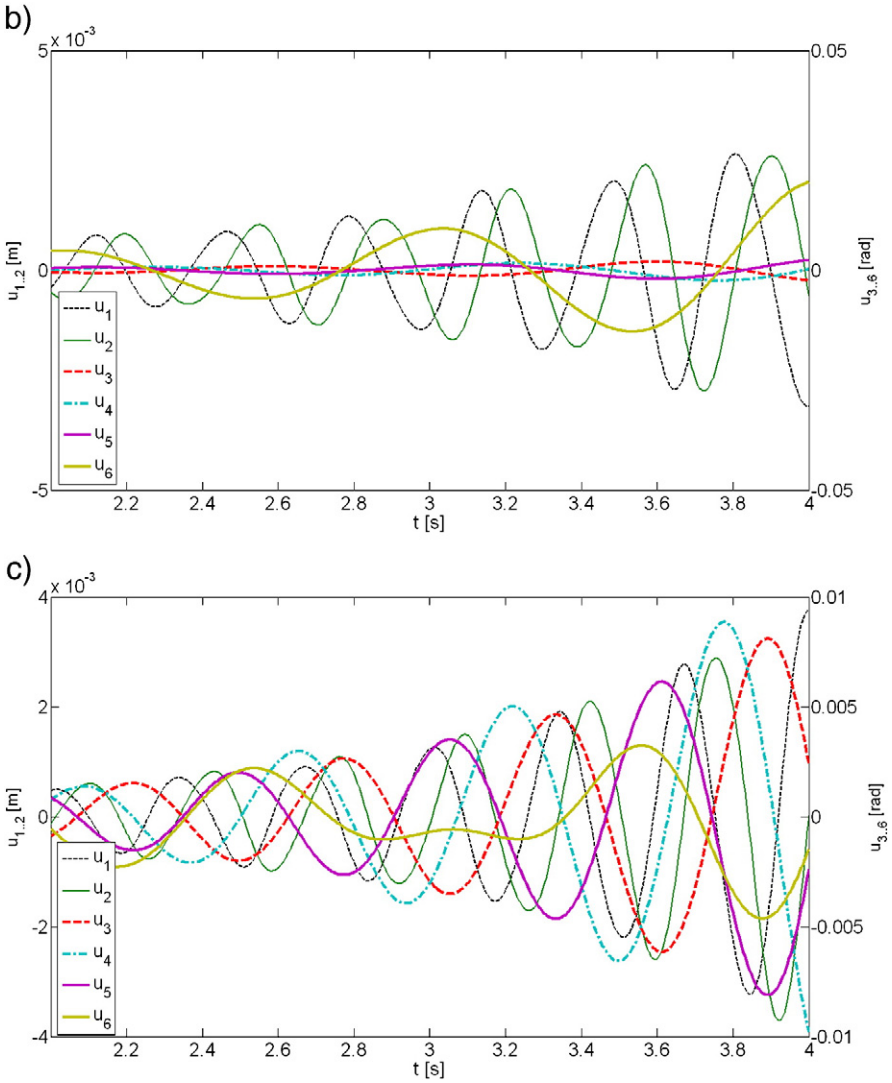

Fig. C1 (*continued*).

References

[1] R.P. Coleman, A.M. Feingold, Theory of self-excited mechanical oscillations of helicopter rotors with hinged blades, NACA Report, 1958, p. 1351.
[2] R.E. Donham, S.Y. Cardinale, I.B. Sachs, Ground and air resonance characteristics of a soft inplane rigid rotor system, J. Amer. Helicopter Soc. 14 (4) (1969).
[3] R.T. Lytwyn, W. Miao, W. Woitch, Airborne and ground resonance of hingeless rotors, J. Amer. Helicopter Soc. 16 (2) (1969).
[4] S.P. Dawson, An experimental investigation of the stability of a bearingless model rotor in hover, J. Amer. Helicopter Soc. 28 (4) (1983).
[5] D.H. Hodges, An aeromechanical stability analysis for bearingless rotor helicopters, J. Amer. Helicopter Soc. 24 (1) (1979).
[6] D. Kunz, Nonlinear analysis of helicopter ground resonance, Nonlinear Analysis Real World Applications 3 (2002) 383–395.
[7] L. Byers, F. Gandhi, Rotor blade with radial absorber, American Helicopter Society 62nd Annual Forum, May 2006 Phoenix.
[8] M. Duchemin, A. Berlioz, G. Ferraris, Dynamic behaviour and stability of a rotor under base excitations, J. Vib. Acoust. 128 (5) (2006) 576–585.
[9] A.H. Nayfeh, D.T. Mook, Nonlinear Oscillations, 2nd ed, John Wiley, 2004, pp. 273–286.
[10] L. Sanches, G. Michon, A. Berlioz, D. Alazard, Modélisation Dynamique d'un Rotor sur Base Flexible (Dynamical Modelling of a Rotor over a Flexible Base), Congrès Français de Mécanique, August 24–28, Marseille, 2009.
[11] J.M. Wang, I. Chopra, Dynamics of helicopters in ground resonance with and without blade dissimilarities, AIAA Dynamics Specialists Conference, April 16–17 Dallas, Texas, 1992.
[12] A. Lazarus, B. Prabel, D. Combescure, A 3D finite element model for the vibration analysis of asymmetric rotating machines, J. Sound Vib. 329 (2010) 3780–3797.
[13] G. Genta, Vibration dynamics and control, Mechanical Engineering Series, Springer, 2009.
[14] R. Dufour, A. Berlioz, Parametric instability of a beam due to axial excitation and to boundary conditions, J. Vib. Acoust. 120 (2008) 461–467.
[15] N.K. Garg, B.P. Mann, N.H. Kim, M.H. Kurdi, Stability of a time-delayed system with parametric excitation, J. Dyn. Syst. Meas. Control 129 (2007) 125–135.
[16] T. Insperger, G. Stepan, Stability chart for the delayed Mathieu equation, Proc. R. Soc. London A 458 (2002) 1989–1998.